1-1-2006

Electron microscope studies of Al-Fe-Si intermetallics in an A1-11 percent alloy

M V. Kral
University of Canterbury

P N H Nakashima
Monash University

D RG Mitchell
ANSTO, dmitchel@uow.edu.au

Electron microscope studies of Al-Fe-Si intermetallics in an A1-11 percent alloy

Abstract

Al-Fe-Si intermetallic particles in both unmodified and highly modified sand-cast eutectic Al-11.7 pct Si alloys were characterized using scanning and transmission electron microscopy, energy-dispersive X-ray spectroscopy, and convergent beam and selected area electron diffraction. The only two Al-Fe-Si intermetallics observed in this particular alloy are (1) “Chinese-script” morphology, consistent with a description of body-centered cubic a-A119Fe4MNSi2 and (2) plate-shaped, consistent with tetragonal d-A1eFeSi2. The authors are unaware of any other characterization of d-A1eFeSi2 using convergent beam electron diffraction (CBED) and selected area diffraction (SAD) techniques.

Keywords

11, intermetallics, a1, alloy, percent, si, studies, fe, al, electron, microscope

Disciplines

Engineering | Physical Sciences and Mathematics

Publication Details

Kral, M. V., Nakashima, P. N H. and Mitchell, D. RG. (2006). Electron microscope studies of Al-Fe-Si intermetallics in an A1-11 percent alloy. Metallurgical and Materials Transactions A: Physical Metallurgy and Materials Science, 37 (6), 1987-1997.

Electron Microscope Studies of Al-Fe-Si Intermetallics in an Al-11 Pct Si Alloy

M.V. KRAL, P.N.H. NAKASHIMA, and D.R.G. MITCHELL

Al-Fe-Si intermetallic particles in both unmodified and highly modified sand-cast eutectic Al-11.7 pct Si alloys were characterized using scanning and transmission electron microscopy, energy-dispersive X-ray spectroscopy, and convergent beam and selected area electron diffraction. The only two Al-Fe-Si intermetallics observed in this particular alloy are (1) ''Chinese-script'' morphology, consistent with a description of body-centered cubic α-$Al_{19}Fe_4MnSi_2$ and (2) plate-shaped, consistent with tetragonal δ-Al_3FeSi_2. The authors are unaware of any other characterization of δ-Al_3FeSi_2 using convergent beam electron diffraction (CBED) and selected area diffraction (SAD) techniques.

I. INTRODUCTION

TOTAL world aluminum smelter production was estimated at 27.3 million tons in 2003 by the U.S. Geological Survey,[1] more than double the production 30 years before. Casting alloys account for 20 pct of aluminum products;[2] of these, eutectic alloys are often selected for their superior casting characteristics.[3] Commercial aluminum alloys always contain small amounts of iron, which can combine with aluminum and silicon to form brittle intermetallic phases that are detrimental to mechanical properties and extrusion characteristics.[4] These intermetallic phases obtain various shapes, and it is generally accepted that plate shapes are most detrimental to mechanical properties such as tensile elongation and fracture toughness.[5]

More than one review of Fe-rich intermetallic phases in Al-Si alloys containing iron has been conducted[6,7,8] to reveal that there are at least 17 different Al-Fe and Al-Fe-Si phases. Some of these phases are metastable, and not all have had atomic coordinates determined. Despite the plethora of possible phases, generally only two of these phases are considered to be common in Al-Si casting alloys. For example, the *Metals Handbook*, vol. 9,[9] describes the two main Al-Fe-Si intermetallic phases found in ''binary'' aluminum-silicon casting alloys such as the British Standard LM6 and Aluminum Association designation 4xx.x alloys. The α phase exhibits a dendritic morphology often called ''Chinese script.'' The other common phase is described as plates or blades and referred to as the β phase. A survey of more recent literature for near-eutectic Al-Si alloys[10–13] shows that plate-shaped phases are generally assumed to be β phase. However, returning to much earlier literature (Phragmen[14] and Mondolfo[5]), there is another phase, termed δ, that also assumes a plate shape and is reported[5] to occur in high-silicon alloys.

It is therefore useful to review what is currently known about these three major intermetallic phases reported in Al-Si casting alloys. First, the α phase is identified perhaps most commonly as Al_8Fe_2Si[15] or generically α-AlFeSi, for examle.[16] There is substantial evidence that the α phase is body-centered cubic, as found by Zheng *et al.*[15] and Skjerpe.[8] The structure of this phase has been described by Cooper[17] as $Al_{19}Fe_4MnSi_2$, space group $Im\bar{3}$, $a = 1.256$ nm. A hexagonal α phase has also been identified.[5] Munson[18] proposed that traces of transition elements such as manganese, chromium, or copper stabilize the cubic phase. Since commercial alloys will always have these elements as impurities or intentional additions, the cubic α phase is of primary interest.

Second, as previously mentioned, plate-shaped precipitates containing iron are most commonly identified in the literature as β-Al_5FeSi or generically as the β phase, for example.[5,10,13,19] However, the most recent investigations[4,20–24] have reached conflicting conclusions regarding the structure and stability of these β-phase precipitates. Carpenter and Le Page describe[21] β-Al_5Fe_2Si as B-face centered orthorhombic with $a = 0.6184$ nm, $b = 0.6250$ nm, $c = 2.069$ nm. Similarly, Zheng *et al.*[22] found the phase to be orthorhombic with $a = 0.618$ nm, $b = 0.620$ nm, $c = 2.08$ nm. However, Murali *et al.*[21] claim that β-Al_5FeSi is monoclinic with $a = 0.5792$ nm, $b = 1.2273$ nm, $c = 4.313$ nm and $\beta = 98.93$ deg. Rømming *et al.*[23] found this phase to be monoclinic with $a = 0.6161$ nm, $b = 0.6175$ nm, $c = 2.0813$ nm and $\beta = 90.42$ deg and fully described the atomic coordinates.

Third, a different plate- or blade-shaped phase containing Fe, Al, and Si has been reported as δ-Al_4FeSi_2, tetragonal with $a = 0.615$ and $c = 0.947$,[25] and was also found by Phragmen.[14] The atomic coordinates of this phase were determined by single crystal X-ray diffraction and described as Al_3FeSi_2 with a space group symmetry of I4/mcm and lattice parameters $a = 0.607$ nm and $c = 0.950$ nm.[26] In the present paper, this phase will be termed δ-Al_3FeSi_2 to carry on the usual Greek-letter designation, but still refer to the more detailed X-ray diffraction of Panday and Schubert.[26]

Alloying additions (*e.g.,* manganese) and/or heat treatments are often applied to counter the undesirable effects of Al-Fe-Si intermetallics.[3] It is has been proposed that a reduced solidification rate,[27] increased strontium additions, and/or the presence of transition elements such as manganese and cobalt[28] will promote the stability of the α phase (which is more compact in shape and therefore more desirable) over the β phase (which is plate-shaped and therefore less desirable).

M.V. KRAL, Associate Professor, is with the Department of Mechanical Engineering, University of Canterbury, P.O. Box 4800, Christchurch, New Zealand. Contact e-mail: milo.kral@canterbury.ac.nz P.N.H. NAKASHIMA, Research Fellow, is with the Department of Materials Engineering, Monash University, Clayton, Victoria 3800, Australia. D.R.G. MITCHELL, Principal Research Scientist, is with the Institute of Materials and Engineering Science, Australian Nuclear Science and Technology Organization, PMB 1 Menai, NSW 2234, Australia.

Manuscript submitted August 10, 2004.

Since there is general agreement that elimination of the plate-shaped phase (perhaps by preferential formation of Chinese-script phase) would result in improved properties of Al-Si alloys, it is critical that intermetallic phases be properly identified so the efficacy of any steps taken can be quantified. Intermetallic phases are often identified in optical or scanning electron microscopes by etching response, morphology, and/or energy-dispersive X-ray spectroscopy (EDS).[7,13,16,19,27,29–35] Morphological classification is unreliable because intermetallic phases may not clearly exhibit their classic Chinese script or plate shape, especially in wrought alloys or cast alloys with eutectic modifiers.[3,5] Less subjective techniques, such as X-ray diffraction or convergent beam electron diffraction, have also been used to further understand the crystallography of these phases.[5,6,14,20–24,26,36–41]

As mentioned, there have been some conflicting reports of crystal structure and morphology of these phases in the literature. Previous work[42] was undertaken to identify these intermetallic phases by the electron backscatter diffraction (EBSD) technique, since EBSD is less ambiguous than metallographic methods and much more convenient than electron diffraction in TEM to survey large numbers of particles. In that work, particles with the Chinese-script morphology always exhibited EBSD patterns consistent with cubic $Al_{19}Fe_4MnSi_2$, space group $Im\bar{3}$, $a = 1.256$ nm.[17] EBSD patterns of the plate-shaped phase were always consistent with tetragonal Al_3FeSi_2, space group I4/mcm, $a = 0.607$ nm and $c = 0.950$ nm,[26] which is sometimes called δ-Al_4FeSi_2[5] but relatively seldom mentioned in the literature. Even so, the identification of relatively small (<200 nm in their smallest dimension) precipitates by EBSD could still be called into question if the precipitates are possibly multiphase composites, such as suggested by Zheng *et al.* for the β phase.[22] EBSD is very useful for identifying known phases that have known atomic coordinates, but EBSD is not sensitive to small differences in lattice parameter (no better than 10 pct) or subtleties to the structure.

The identification of plate-shaped particles as tetragonal δ-Al_3FeSi_2 appears to be unusual, and the authors are unaware of any other detailed electron microscopy study of the δ-Al_3FeSi_2 phase. The present work was therefore

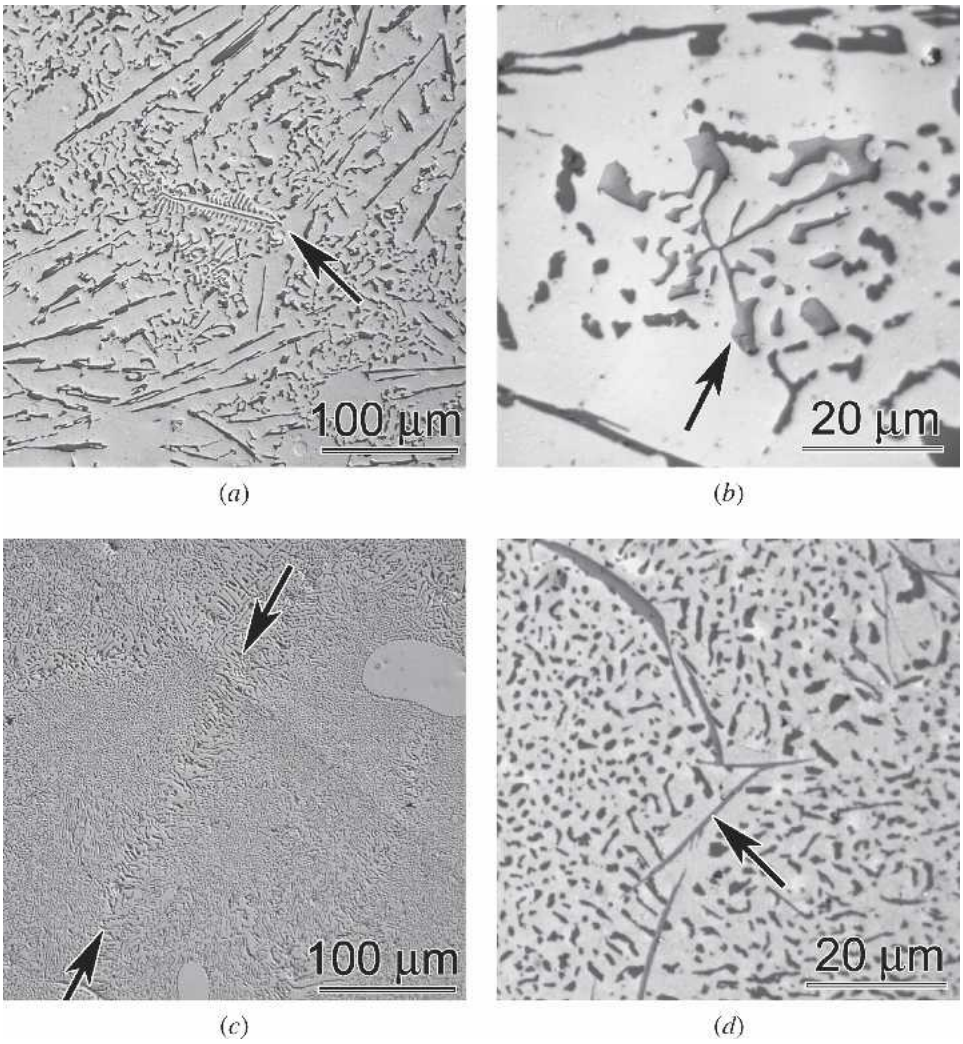

Fig. 1—Optical micrographs of intermetallic phases in the Al-11 pct Si alloy. In unmodified alloys (*a*) and (*b*), script particles are shown in light-gray aluminum matrix along with coarse dark-gray silicon plates. In modified alloys (*c*) and (*d*), plate-shaped particles appear at boundaries between eutectic colonies (*e.g.,* between arrows in (*c*)) in light-gray aluminum matrix along with highly refined, dark-gray modified silicon eutectic.

performed to investigate Al-Fe-Si intermetallic precipitates in an Al-11.7 pct Si alloy with TEM using convergent beam electron diffraction (CBED) and selected area diffraction (SAD) techniques.

II. EXPERIMENTAL PROCEDURES

Samples were taken from 270-kg production melts of a commercial aluminum-silicon eutectic casting alloy at CWF Hamilton Ltd., Christchurch, New Zealand. The alloy was supplied by the Comalco Tiwai Point (Invercargill, New Zealand) smelter and was produced to meet Australian Standard 1874-EA401, with an initial composition of Al-11.7Si-0.16Fe-0.13Mn-0.01Mg (wt pct). The alloy was held at 750 °C for approximately 12 hours and degassed for 300 seconds with dry nitrogen prior to casting. During the degassing process, 300 g of Al-5 pct Ti-1 pct B and Al-10 pct Sr master alloy rods were added to give an Sr content of 0.06 wt pct. Further details of alloy preparation were given previously.[42]

Based on previous observations that unmodified alloys exhibit relatively large script Al-Fe-Si particles and that sodium- and strontium-modified alloys frequently exhibit plate-shaped Al-Fe-Si particles, samples of each alloy type was chosen for the present analysis. The unmodified samples were obtained from the melt just prior to degassing. Samples of modified alloys were taken approximately 8000 seconds after Sr additions or 600 seconds after Na additions. Cross-sections for optical and scanning electron microscopy were cut from the central section of the tensile test bars after tensile testing was completed. The cooling rate for all samples was similar, all being taken from the same regions of sand-cast samples, all cast near the same temperature into the same shape of mold. SEM of polished sections was performed using a JEOL JSM6100 equipped with an Oxford eXL EDS system and an HKL Nordlys II EBSD system with Channel 5 system software. A typical procedure would be to obtain an SEM image of a particle of interest, obtain an EDS spectrum, and then tilt to the 70-deg orientation required for EBSD pattern acquisition, keeping the same particle in view during the tilt.

Specimens for TEM studies were prepared in two different ways. Conventional 3-mm-diameter samples were punched from 0.3-mm-thick cross-sections and ground to

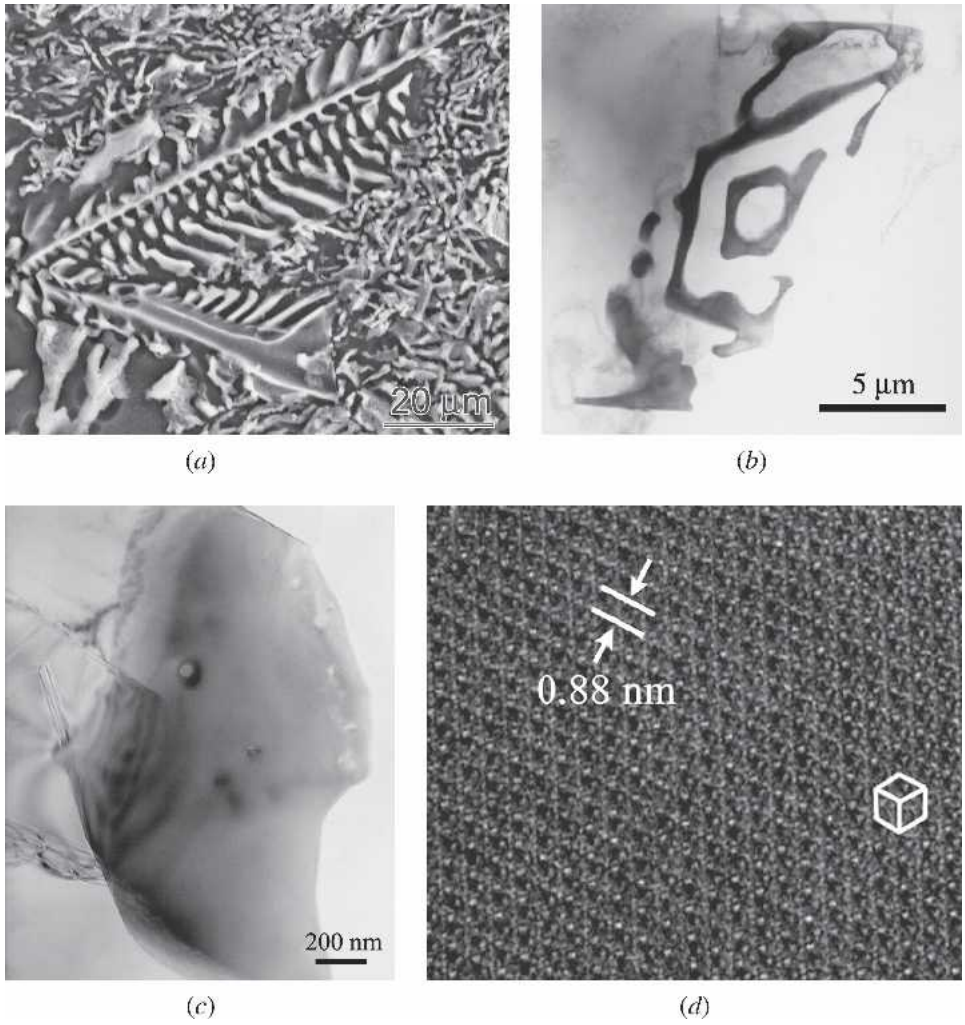

Fig. 2—The morphology of script particles in an unmodified alloy is revealed by (*a*) a scanning electron micrograph of a deep-etched specimen, and (*b*)[55] and (*c*) transmission electron micrographs and (*d*) a lattice image from the particle shown in (*c*) near ⟨111⟩ showing a projection of the unit cell and spacing of the {110}.

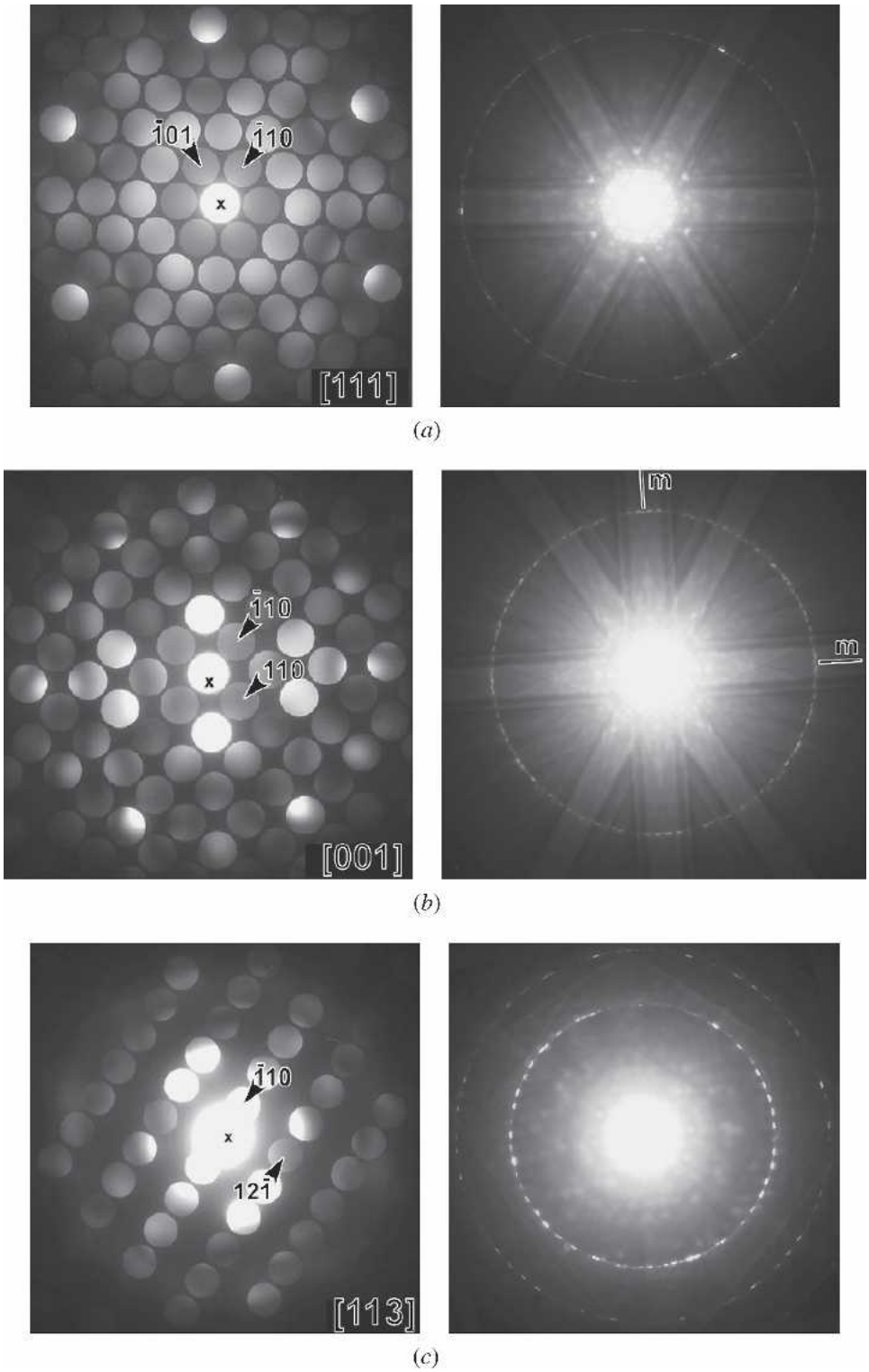

Fig. 3—Convergent beam electron diffraction patterns from the same particle as shown in Figure 2(c), showing both ZOLZ and HOLZ patterns for (*a*) $z = [111]$[58], (*b*) $z = [100]$ and (*c*) $z = [113]$. Crosses show the position of the exact zone axis and are coincident but not always exactly concentric with the central beam (000), which is not labeled.

approximately 0.1 mm in thickness. A Gatan Model 656 Dimple Grinder and a Model 691 Precision Ion Polishing System were used to produce thin foils. Alternatively, particles were extracted from the matrix by electrolytic dissolution in NaOH, placed on a Formvar-coated copper grid, and subsequently coated with carbon. TEM was performed on three different microscopes. For the Chinese-script phase analysis, all CBED results were obtained on a Philips CM20 (operated at 160 kV and 200 kV) and high-resolution images on a JEOL 2011 (operated at 200 kV), both equipped

with an energy-dispersive X-ray spectrometer, at Monash University, Melbourne, Australia. Some analysis was performed using an Hitachi H600 TEM (equipped with a Kevex energy dispersive X-ray detector and Moran Scientific analysis software) operating at an accelerating voltage of 100 kV at the University of Canterbury, Christchurch, New Zealand. CBED and quantitative EDS were performed using a JEOL FX2 TEM operated at both 200 and 160 kV equipped with a calibrated Oxford energy-dispersive X-ray spectrometer and analysis system.

III. RESULTS AND DISCUSSION

Figure 1 shows the distribution and morphology of Chinese-script particles in an unmodified sand-cast Al-11 pct Si alloy and plate-shaped particles in same alloy modified with either sodium or strontium. As shown in Figures 1(a) and (b) (and also Figures 2(a) and (b)), the Chinese-script particles exhibit the morphology that has led to vivid descriptions such as ''fossil-shaped.'' Chinese-script particles were often observed within regions of relatively refined

Table I. Convergent Beam Symmetries from the Script Phase

Zone Axis	Observed Symmetry in Zero-Order Zone	WP Symmetry	Possible Diffraction Groups	Possible Point Groups
[111]	6	3	6, 6_R, 61_R	6, $\bar{3}$, m3, 6/m
[001]	2mm	2mm	2mm, $2mm1_R$	mm2, 6m2, mmm, 4/mmm, 23, m3, m3m
[113]	2	1	2_R	mm2, 6m2, mmm, 4/mmm, 23, m3, m3m

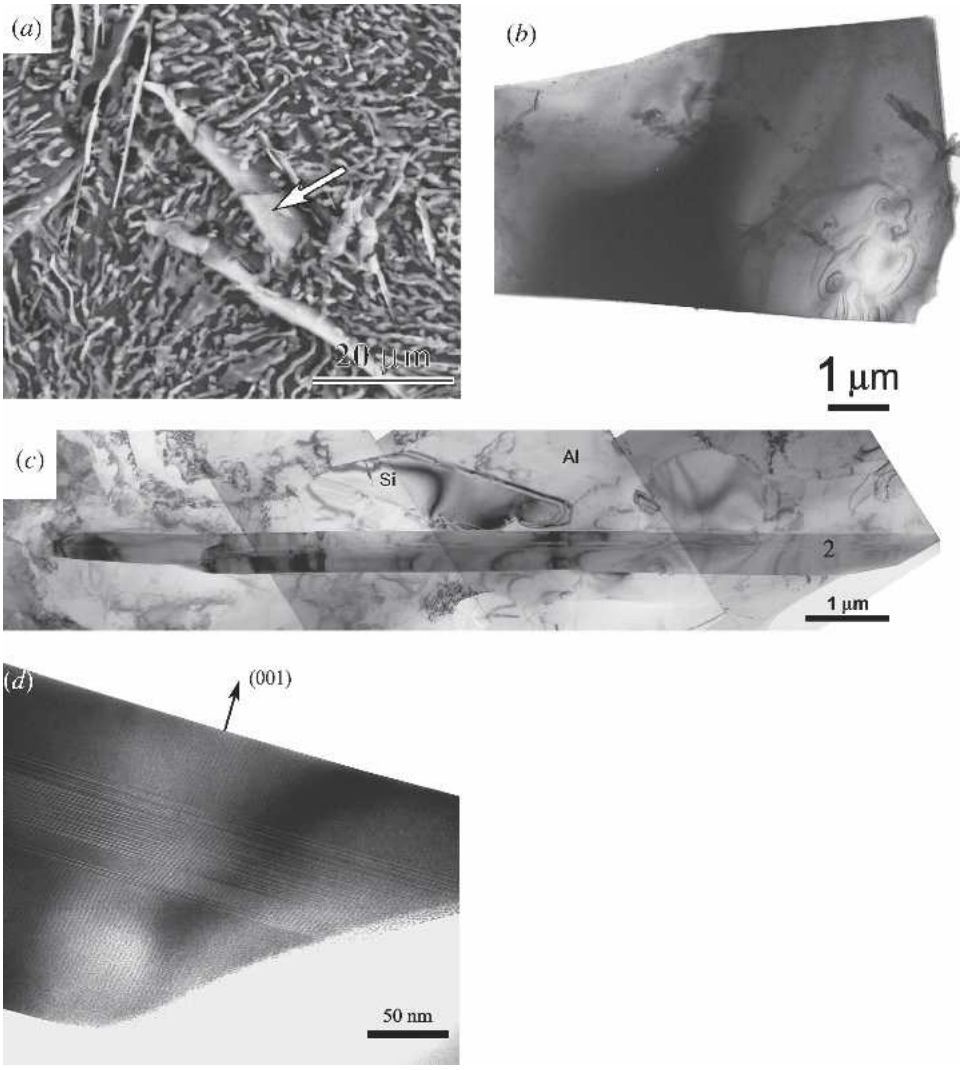

Fig. 4—(*a*) An SEM image of a deep-etched sample showing typical plates. (*b*) A bright-field TEM image of an extracted plate revealing the plate 3D morphology. (*c*) A montage of bright-field TEM images shows the typical appearance of a plate (designated ''2'') in cross-section. (*d*) A higher-magnification TEM image of a plate-shaped particle shows the faults often observed and that the normal to the broad face of the plate is parallel to (001).

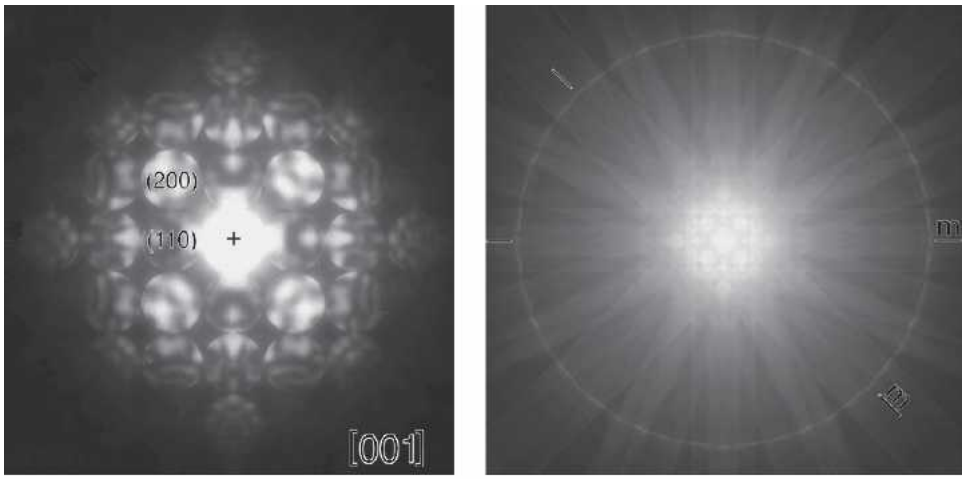

(*a*)

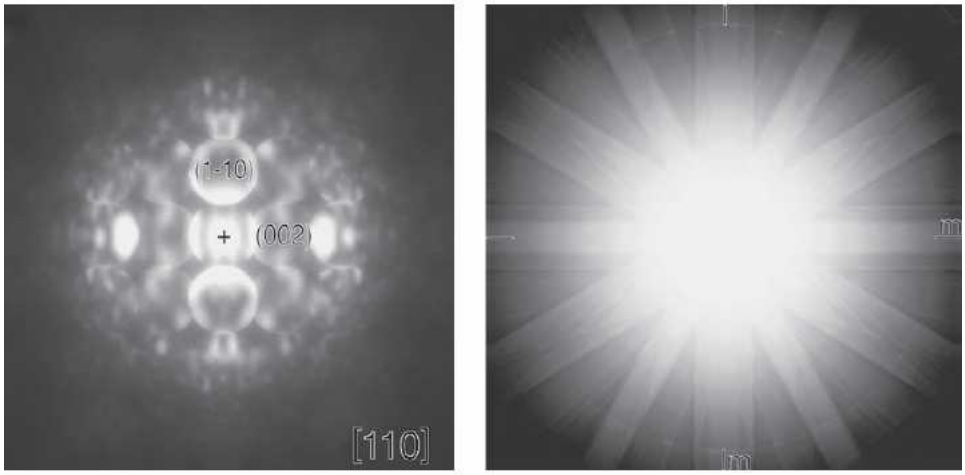

(*b*)

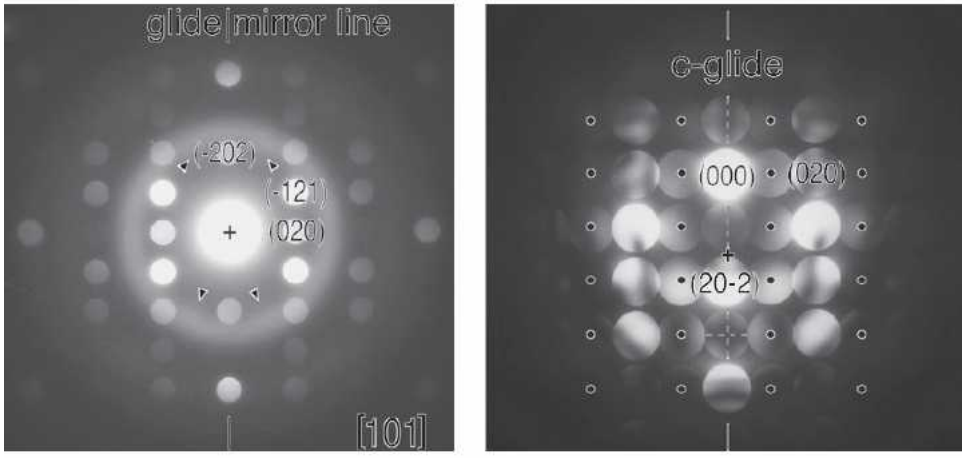

(*c*)

Fig. 5—Convergent beam electron diffraction patterns from various plate-shaped particles, showing both ZOLZ and HOLZ patterns for (*a*) $z = [001]$ and (*b*) $z = [110]$. Only the ZOLZ is required in (*c*) to show the Gjønnes-Moodie lines in the projection along the [101] zone, indicative of the c-glide in the structure. The left side of (*c*) is from a very thin region of specimen where the oxide layer gives rise to the diffuse rings concentric with the central beam. Arrows indicate the very faint extra reflections, which are almost invisible but detectable on the negatives. The right pattern in (*c*) is from a thicker region with the extra reflections not expected in the space group I4/mcm, marked with dots. The higher frequency of the intensity distribution reveals the Gjønnes-Moodie lines (marked with dashed lines) characteristics of the c-glide in the structure. The line in the $(10\bar{1})$ reflection is difficult to see due to the diffuse background caused by inelastic scattering of electrons from the specimen. Again, small crosses locate the exact zone axis and in all cases except the off-axis pattern in (*c*), the crosses are also coincident with (000).

silicon particles, perhaps modified by high local solidification rates or high impurity concentration. The Chinese-script phase was the most common intermetallic phase in unmodified alloys; plate-shaped intermetallic phases were observed much less often in comparison.

Plate-shaped particles tend to appear at eutectic colony boundaries, such as between the arrows in Figure 1(c). The plate-shaped particles often obtain a curved morphology (Figure 1(d)), although, as will be shown later, the broad faces of individual plates are planar at higher magnification in TEM specimens. This curved blade-shaped appearance at the optical microscopy level may be due to deformation during the solidification process, particles impinging upon one another, and/or cross-sectioning effects. In modified alloys, the plate-shaped phase was by far the most common phase other than aluminum and silicon.

A. *Crystallography of the Chinese-Script Phase*

As mentioned earlier, Chinese-script particles exhibit EBSD patterns[42] that are consistent with body-centered cubic $Al_{19}Fe_4MnSi_2$, space group $Im\bar{3}$, $a = 1.256$ nm, as described by Cooper.[17] This phase, commonly called the α phase in the literature, is easily located in the thin areas of the TEM foil by its generally dark appearance in comparison with the aluminum matrix and eutectic silicon due to atomic number contrast[43] (*e.g.,* Figure 2(b)). A series of CBED patterns was obtained at different zone axes in the same precipitate, as shown in Figure 3, to identify the space group. Figure 3(a) is a CBED pattern taken along the $\langle 111 \rangle$ zone with the zero-order Laue zone (ZOLZ) pattern (at left), showing sixfold symmetry in the projected structure. The whole pattern (at right), including higher-order Laue zones (HOLZ), shows that the three-dimensional crystal structure possesses only a threefold axis along $\langle 111 \rangle$, which is typical of many cubic systems. In combination, the symmetry elements in this pattern suggest a diffraction group of 6_R.[44,45] Continuing to Figure 3(b), the perpendicular mirror lines observed in both the ZOLZ and whole patterns give two possible diffraction groups, 2mm or $2mm1_R$.[44,45] Figure 3(c) shows only twofold symmetry in the ZOLZ pattern (which represents the projected crystal symmetry). This implies the 2_R diffraction group.[44,45] Turning to the tables developed by Buxton *et al.*[46] and shown in Reference 44, the only crystal point group that can give rise to the set of diffraction groups, 6_R, 2mm or $2mm1_R$ and 2_R, is m3 in a cubic crystal. This analysis is summarized in Table I. Three space groups are therefore possible: $Pm\bar{3}$ $Fm\bar{3}$ or $Im\bar{3}$.

The absolute space group determination makes use of Figures 3(b) and (c), where the basis vectors in the patterns from $\langle 001 \rangle$ and $\langle 113 \rangle$ are labeled. The $(\bar{1}10)$ reflection is present in both patterns but, regardless of space group, would always appear as the shortest vector at the $\langle 113 \rangle$ zone. This proves that the shortest vector seen at the $\langle 001 \rangle$ is also $(\bar{1}10)$ (due to the same length of the marked vectors in the $\langle 113 \rangle$ and $\langle 001 \rangle$ patterns taken at the same camera length), eliminating the possibility of $Pm\bar{3}$ since (100) would be the shortest symmetry allowed scattering vector.[47] To distinguish between $Fm\bar{3}$ and $Im\bar{3}$, the $\langle 113 \rangle$ pattern has $(12\bar{1})$ as its second basis vector. This is allowed only in $(Im\bar{3})$[47] and thus leads to the conclusion that the Chinese-script phase indeed conforms to the determination of Cooper[17] for $Al_{19}Fe_4MnSi_2$. A high-resolution TEM image of the phase along a $\langle 111 \rangle$ direction shows a projection of the cubic unit cell and {110} interplanar spacings are consistent with the predicted spacings based on the published lattice parameter and structure of $Al_{19}Fe_4MnSi_2$. Very similar results for the α phase have been described in a direct chill-cast aluminum of commercial purity[8] as well as a precipitation-hardened Al-7 pct Si casting alloy containing beryllium.[15] The α-$Al_{19}Fe_4MnSi_2$ designation is therefore an accurate crystallographic representation of the Chinese-script phase found in the present cast eutectic Al-Si alloys.

B. *Crystallography of the Plate-Shaped Phase*

In modified alloys, particles with the plate- or blade-shaped morphology (Figure 4) are much more commonly found than the script α phase. These particles can be tens of microns in length and width and up to ~ 0.5 μm in thickness. Trace analysis showed that the plate broad face is approximately planar and parallel to (001). As illustrated in Figure 4(d), plates sometimes contain planar defects that are parallel to their broad faces.

As mentioned previously, EBSD patterns[42] of plate-shaped precipitates in the present alloy were always consistent with tetragonal Al_3FeSi_2.[26] CBED patterns were obtained from different zone axes as shown in Figure 5 to investigate whether those results were accurate and to determine the space group of this material. Following a similar approach applied to the α-phase, Figure 5(a) shows CBED patterns taken along the [001] zone with 4mm symmetry in both the ZOLZ (left) and HOLZ (right) patterns. In Figure 5(b), the [110] zone axis pattern exhibits 2mm symmetry in both the ZOLZ and HOLZ. Figure 5(c) is comprised of two patterns from the [101] zone, one on-axis and the other with the incident beam tilted along the glide/mirror line in the crystal structure that is evident from these patterns. The patterns shown in Figure 5 will now be analyzed in assessing the space group of the plate-shaped phase.

The patterns from [001] and [110] alone are all that is necessary to conclude the structure is body-centered tetragonal with a point group of 4/mmm. Firstly, the lengths of the basis vectors and radii of the first order Laue zones (FOLZ) in both patterns are consistent with the body-centered tetragonal structure proposed by Panday and Schubert.[26] Having established a body-centered tetragonal lattice from Figure 5(a) and (b), the point group can be more easily determined. The symmetry elements in the [001] pattern of Figure 5(a) suggest diffraction groups of either 4mm or $4mm1_R$.[44,45,46] Figure 5(b), yields only one possible diffraction group at the [110] zone, $2mm1_R$.[44,45,46] The group $2mm1_R$ cannot coexist with 4mm, implying that the diffraction group observed in the pattern from [001] is $4mm1_R$.[45,46] Therefore, the point group in the present plate-shaped phase can only be 4/mmm.

While a point group conclusion of 4/mmm is in agreement with Panday and Schubert,[26] further work is required to conclude a particular space group. Patterns along the [101] zone should exhibit evidence of the c-glide if we

assume the I4/mcm space group to be correct.[48] Figure 5(c) (left) shows the [101] ZOLZ pattern from a very thin region of the plate-shaped phase in the specimen. The uniformity of the illumination and the strong amorphous signal from the unavoidable oxide layer on the specimen attest to the thinness of the diffracting crystal. Worth noting are the missing odd orders of the (h0h) reflections. Dynamic scattering (multiple scattering) should yield intensity in these reflections, in the absence of a c-glide, due to an infinite number of multiple scattering pathways to these reflections. A single example is (000) → ($\bar{1}21$) → ($\bar{1}01$). In this case, the scattering amplitudes for the ($\bar{1}21$) and ($0\bar{2}0$) vectors as a dynamic diffraction pathway to the ($\bar{1}01$) are non-zero. However, summing over all possibilities in the presence of a glide will yield overall extinctions in these reflections as per Gjønnes and Moodie[49] and as first observed by Goodman and Lehmfuhl.[48,50] In the case where the crystal is very thin, the odd ($\bar{h}0h$) reflections will be completely absent so the pattern in Figure 5(c) (left) shows evidence of the c-glide in the structure. Another aspect of this pattern is that extra reflections along the (0k0) vector are just beginning to appear as marked with arrows in the pattern. This suggests some reduction in symmetry, possibly due to stacking faults or twinning alluded to earlier, since these reflections would otherwise be forbidden (dynamically and kinematically).

Figure 5(c) (right) is a pattern also along the [101] zone, but taken from a significantly thicker region of the same crystal that yielded the [101] pattern in Figure 5(c) (left). In addition, the incident beam has been tilted slightly off-axis along the glide mirror line such that the ($30\bar{3}$) reflection satisfies the Bragg condition. The higher frequency of the intensity distribution due to the greater crystal thickness results in extinction lines in the odd ($\bar{h}0h$) reflections, coincident with the glide mirror line. In the pattern taken from the thinner region, Figure 5(c) (left), these extinction lines are broad enough to make the reflections completely disappear. These extinction lines are known as Gjønnes–Moodie lines[45,48,49] and the cross that appears in the Bragg satisfied ($30\bar{3}$) reflection is further conclusive evidence of the c-glide in the structure.[45,48,49]

The reflections marked with dots in Figure 5(c) (right) should not be present in a body-centered tetragonal structure but can be explained if the centering of the structure were P instead if I. The additional reflections that have appeared at the greater crystal thickness and that started to appear only very weakly in the first pattern from the thinner region, are most likely due to a combination of stacking faults (as observed in images and previously commented on) and possible twinning. The only aspect that seems to change is the appearance of the reflections that are forbidden in the I4/mcm space group but are allowed in P4/mcm. Otherwise, the symmetry of the patterns does not change, the c-glide and point group of 4/mmm remaining invariant. Similar observations of the appearance of extra reflections were made at other zone axes such as [100] and [110], not included here for the sake of brevity. A doubling in the number of reflections without any change in the observed symmetries along these zone axes was also recorded.

In summary, the CBED study embodied in Figure 5 clearly shows that the highest crystal symmetry of the

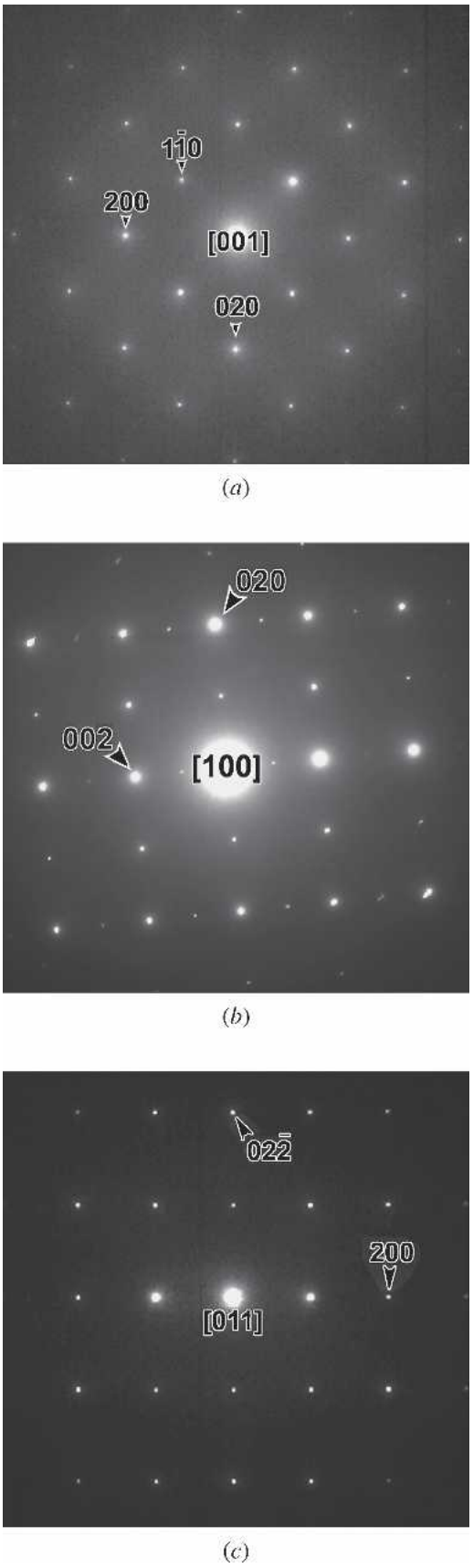

Fig. 6—Experimental selected area diffraction patterns from the particle shown in Figure 4(c), (*a*) z = [001], (*b*) z = [100], and (*c*) z = [011] indexed assuming tetragonal Al_3FeSi_2, a = 0.607 nm and c = 0.950 nm.

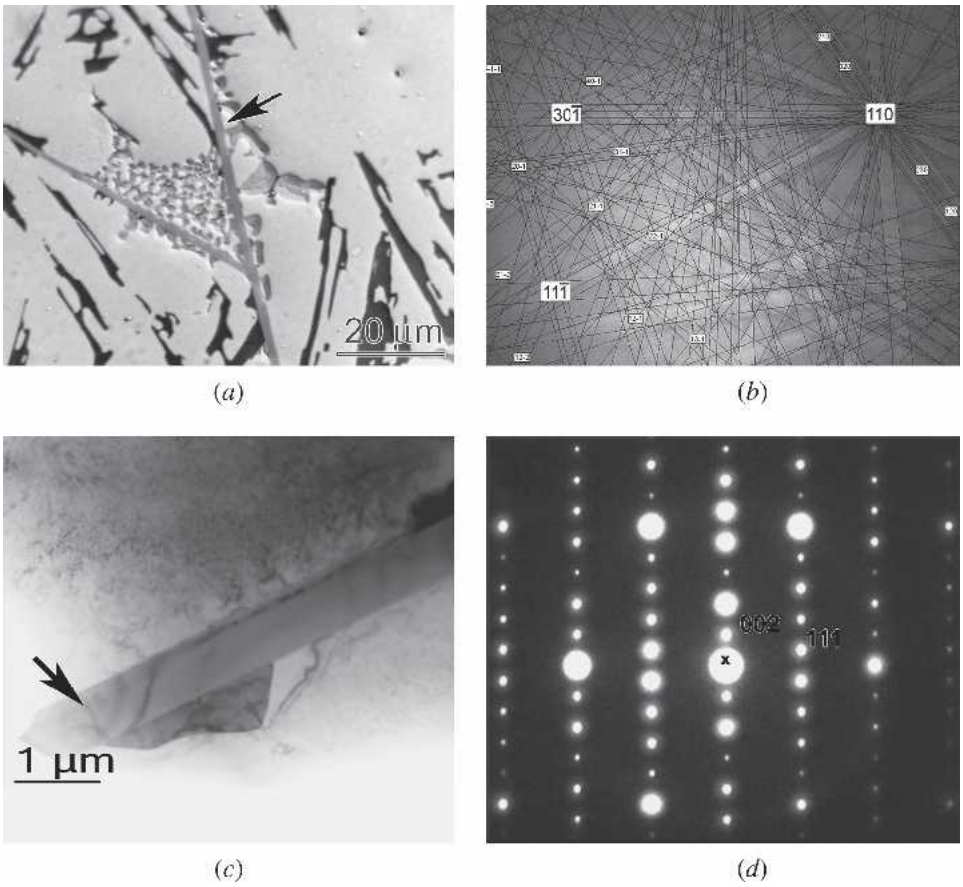

Fig. 7—Characterization of the β-$Al_9Fe_2Si_2$ phase in (*a*) optical micrograph, (*b*) EBSD pattern indexed as $Al_9Fe_2Si_2$, (*c*) bright-field TEM image of a β-phase plate, and (*d*) selected area diffraction of a β-phase plate along [110].

plate-shaped phase has the space group I4/mcm as determined by Panday and Schubert.[26] However, the average symmetry of the bulk material involves a change in the centering type from I to P resulting in a symmetry reduction to space group P4/mcm.

A series of selected area electron diffraction (SAD) patterns was obtained over a large range of tilts from two examples of extracted plate-shaped particles. Figure 6 shows SAD patterns from the ⟨001⟩, ⟨100⟩, and ⟨011⟩ zone axes. Extracted particles exhibited interplanar spacings, based upon camera constants calibrated from single crystal silicon, within 1 pct of the published values for tetragonal Al_3FeSi_2 (a = 0.607 nm, c = 0.950 nm),[26] further confirming the tetragonal unit cell. The angles between zones and angles between planes within each zone are also consistent with tetragonal Al_3FeSi_2. However, some reflections that were actually observed (*e.g.,* (001), (012) and (010) in the [100] pattern)[47] are anomalous with the space group I4/mcm and echo the CBED observations of a symmetry reduction to P4/mcm. SAD patterns represent a much larger probed region of the specimen and are much more indicative of the averaged structure, while the focused probes in CBED allow much smaller volumes of crystal to be analyzed including perfect, defect free regions of a specimen. The combined CBED and SAD results therefore yield the same conclusion stated previously: the δ-phase ultimately has an I4/mcm space group, as per Panday and Schubert,[26] in a perfect crystal region, which reduces to the lower symmetry P4/mcm averaged structure in the bulk of the plate-shaped phase found in the present case eutectic Al-Si alloys.

For comparison, the typical appearance of the β-$Al_9Fe_2Si_2$ phase from a die-casting alloy (known as LM24 with composition in this case Al-9 pct Si-1.3 pct Fe-3.3 pct Cu-0.4 pct Mn) is shown in Figure 7. Optical microscopy of the β phase (Figure 7(a)) compared with images of the δ phase (Figures 1(c) and (d)) show that in this case the β phase is generally coarser and exhibits none of the curved blade-shaped appearance in optical microscopy that has been noted for the δ phase in the present work. EBSD patterns (*e.g.,* Figure 7(b)) of several particles such as shown in Figure 7 were clearly indexed as the phase identified by Rømming *et al.* as monoclinic β-$Al_9Fe_2Si_2$.[23] Figure 7(c) shows the bright-field image of one of these particles and Figure 7(d) shows a selected area diffraction pattern indexed as [110], appearing nearly identical to Figure 2(d) in Rømming *et al.*[23] and Figure 3(e) in Hansen *et al.*[24]

A standardless EDS analysis of the particles in TEM allows only a semiquantitative comparison of the two phases. A summary of data taken from three different particles indexed as δ phase and four particles indexed as β phase is provided in Table II. These data show an approximately 1:1 (Fe):Si ratio for the β phase and approximately 1:2 (Fe):Si ratio for the δ phase, which is in general agreement with the accepted stoichiometries of these phases. It is

interesting to note the manganese content in the δ phase, even though manganese is often reported to stabilize the α phase over the δ phase. At this point, even though there is substantial evidence that manganese additions enhance mechanical properties in aluminum alloys,[3,48] there is no reason from the present work to believe that this occurs by altering the morphology of the plate-shaped Al-Fe-Si phases in the Al-11.7 pct Si alloy, as suggested in Reference 3. The effect of manganese additions has been studied extensively for 6xxx alloys,[4,49] where Mn apparently promotes the formation of the α phase over the β phase. The δ phase in Al-11.7 pct Si may interact differently with Mn, however, as compared to the monoclinic or orthorhombic β phases reported in other aluminum alloys. Furthermore, Mn additions did not appear to promote the stability of the α phase in the present Na- and Sr-modified alloys, since plate-shaped particles containing Mn were abundant and script particles were rarely observed. Further work is therefore required to determine the mechanisms by which mechanical properties are influenced when Mn additions are made to Al-Si alloys and whether or not Mn stabilizes the α phase in Al-Si alloys with eutectic modifiers.

The present work, in alloys that are similar in composition to alloys studied by other researchers,[10,13,19,31] indicates that the δ phase may be misidentified as β phase at least in near-eutectic Al-Si casting alloys, since the morphology and stoichiometry are similar.[7,10,13,19,50,51] One possible source of confusion is that in alloys with significantly different compositions and processing conditions, such as the wrought 6xxx aluminum alloys, the main Fe-bearing intermetallic phases are also described as a Chinese-script α phase and a plate-shaped β phase. It appears that the α phase is the same in this Al-11.7 pct Si alloy as the one found in 6xxx alloys[4,49] as well as Al-7 pct Si alloys.[15] However, as mentioned previously, there is no such general agreement regarding the β phase. Inaccurate identification could arise from past researchers' tendency to categorize phases based on their shape and/or composition. Generic descriptions such as those given in the *Metals Handbook*[9] may be problematic, since many researchers will apply these generalizations by default without any direct evidence.

The results of this TEM-based electron diffraction study support the previous SEM-based EBSD study on this Al-11.7 pct Si alloy. Generally, it is clear that EBSD and CBED and/or SAD can be very useful in combination. Once the presence and identity of a known phase is suggested by EBSD, identification can be confirmed via TEM (if necessary) and then EBSD can be used to rapidly identify large numbers of particles in bulk specimens. This would be especially useful when studying the effects of alloying additions on the stability of intermetallic phases in wrought aluminum alloys, for example.[34,52,53,54]

Table II. Average Composition of Plate-Shaped Al-Fe-Si Intermetallics

	Al (At. Pct)	Si	Mn	Fe	Fe + Mn
δ-Al_3FeSi_2	65.8	20.1	2.9	11.2	14.1
β-$Al_9Fe_2Si_2$	61.2	19.7	2.5	16.6	19.2

IV. CONCLUSIONS

Al-Fe-Si intermetallic particles in cast eutectic Al-Si alloys are usually categorized by morphology and/or EDS, and relatively little work has been done previously to identify these particles by crystallographic analysis. The results of an earlier EBSD survey of a large number of Al-Fe-Si particles in an Al-11 pct Si alloy[42] were supported by the present electron diffraction study of thin foil specimens of the same alloys. Intermetallic particles with the Chinese-script morphology are clearly consistent with α-$Al_{19}Fe_4MnSi_2$ (cubic $Im\bar{3}$) Electron diffraction patterns from plate-shaped particles can be usefully indexed as a tetragonal unit cell with $a = 0.607$ nm, $c = 0.950$ nm, and CBED analysis indicates a point group symmetry of 4/mmm with a space group of I4/mcm in regions of perfect crystal and with a space group that reduces to P4/mcm when the structure is averaged over a larger volume containing defects typical of the bulk of the plates.

ACKNOWLEDGMENTS

M.V. KRAL gratefully acknowledges Professor Barry Muddle of the Monash University School of Physics and Materials Engineering for financial support and access to the Monash SPME electron microscopy center while on sabbatical leave from Canterbury. Samples were kindly provided by Mr. Hamish McIntyre. The idea for this research evolved during Technology New Zealand TIF project HAMX0201 with CWF Hamilton and Company Ltd, Christchurch, New Zealand. Partial support was provided through a grant from the Australian Institute of Nuclear Science and Engineering (AINSE, project number AINGRA05221) for use of facilities at the Australian Nuclear Science & Technology Organization (ANSTO).

REFERENCES

1. P.A. Plunkert: "Aluminum, Mineral Commodity Summary". In *U.S. Geological Survey, Mineral Commodity Summaries*, 2004.
2. I.J. Polmear: *Light Alloys*, Edward Arnold (Publishers) Ltd., London, U.K., 1981.
3. J.E. Hatch: *Aluminum, Properties and Physical Metallurgy*, American Society for Metals, Metals Park, OH, 1984.
4. M.H. Mulazimoglu, A. Zaluska, J.E. Gruzleski, and F. Paray: *Metall. Mater. Trans.*, 1996, vol. 27A (4), pp. 929-36.
5. L.F. Mondolfo: *Aluminum Alloys: Structure and Properties*, Butterworths and Co., Ltd., London, U.K., 1976.
6. V.G. Rivlin and G.V. Raynor: *Int. Metall. Rev.*, 1981, vol. 3, pp. 133-52.
7. S. Yaneva, N. Stoichev, Z. Kamenova, and S. Budurov: *Z. Metallkd.*, 1984, vol. 75 (5), pp. 395-98.
8. P. Skjerpe: *Metall. Trans.*, 1987, vol. 18A, pp. 189-200.
9. R.H. Stevens, ed.: *Aluminum Alloys*, ASM International, Materials Park, OH, 1985.
10. X. Cao and J. Campbell: *Metall. Mater. Trans.,* 2004, vol. 35 (5), pp. 1425-35.
11. S.G. Shabestari: *Mater. Sci. Eng.*, 2004, vol. 383, pp. 289-98.
12. C.M. Dinnis, J.A. Taylor, and A.K. Dahle: *Scripta Mater.*, 2005, vol. 53 (8), pp. 955-58.
13. S.-N. Yie, S.-L. Lee, Y.-H. Lin, and J.-C. Lin: *Mater. Trans., JIM*, 1999, vol. 40 (4), pp. 294-300.
14. G. Phragmén: *J. Inst. Metals*, 1950, vol. 77, pp. 489-552.
15. J.G. Zheng, R. Vincent, and J.W. Steeds: *Philos. Mag.*, 1999, vol. 79 (11), pp. 2725-33.
16. L.A. Narayanan, F.H. Samuel, and J.E. Gruzleski: *Metall. Mater. Trans.,* 1995, vol. 26A (8), pp. 2161-74.
17. M. Cooper: *Acta Crystallogr.*, 1967, vol. 23, pp. 1106-07.

18. D. Munson: *J. Inst. Metal.*, 1967, vol. 95, pp. 217-19.
19. S.G. Shabestari and J.E. Gruzleski: *Metall. Mater. Trans.*, 1995, vol. 26A (4), pp. 999-1006.
20. G.J.C. Carpenter and Y. Le Page: *Scripta Metall. Mater.*, 1993, vol. 28, pp. 733-36.
21. S. Murali, T.N.G. Row, D.H. Sastry, K.S. Raman, and K.S.S. Murthy: *Scripta Metall. Mater.*, 1994, vol. 31 (3), pp. 267-71.
22. J.G. Zheng, R. Vincent, and J.W. Steeds: *Philos. Mag.*, 2000, vol. 80 (2), pp. 493-500.
23. C. Rømming, V. Hansen, and J. Gjonnes: *Acta Crystallogr.*, 1994, vol. 50B, pp. 307-12.
24. V. Hansen, B. Hauback, M. Sundberg, C. Rømming, and J. Gjønnes: *Acta Crystallogr.*, 1998, vol. 54B, pp. 351-57.
25. W. Janiche: *Aluminium Archiv*, 1936.
26. P.K. Panday and K. Schubert: *J. Less-Common Metals*, 1969, vol. 18, pp. 175-202.
27. O. Vorren, J.E. Evensen, and T.B. Pedersen: *AFS Trans.*, 1984, vol. 92, pp. 459-66.
28. A. Couture: *AFS Int. Cast Metals J.*, 1981, vol. 6 (4), pp. 9-17.
29. B. Closset and J.E. Gruzleski: *Metall. Trans.*, 1982, vol. 13A, pp. 945-51.
30. S. Murali, K.S. Raman, and K.S.S. Murthy: *Mater. Sci. Eng.*, 1992, vol. A151, pp. 1-10.
31. A.N. Lakshmanan, S.G. Shabestari, and J.E. Gruzleski: *Z. Metallkd.*, 1995, vol. 86 (7), pp. 457-64.
32. A.M. Samuel, F.H. Samuel, and H.W. Doty: *J. Mater. Sci.*, 1996, vol. 31 (20), pp. 5529-39.
33. F.H. Samuel, P. Ouellet, A.M. Samuel, and H.W. Doty: *Metall. Mater. Trans.*, 1998, vol. 29A (12), pp. 2871-84.
34. F.H. Samuel, A.M. Samuel, H.W. Doty, and S. Valtierra: *Metall. Mater. Trans.*, 2001, vol. 32A, pp. 2061-75.
35. M. Ravi, U.T.S. Pillai, B.C. Pai, A.D. Damodaran, and E.S. Dwarakadasa: *Metall. Mater. Trans.*, 2002, vol. 33A (2), pp. 391-400.
36. K. Robinson: *Acta Crystallogr.*, 1952, vol. 5, pp. 397-403.
37. D. Munson: *J. Inst. Metal.*, 1967, vol. 95, pp. 217-19.
38. L.A. Bendersky, A.J. McAlister, and F.S. Biancaniello: *Metall. Trans.*, 1988, vol. 19A, pp. 2893-900.
39. J.E. Tibballs: *Key Eng. Mater.*, 1990, vol. 44, pp. 233-46.
40. T. Turmezey, V. Stefaniay, and A. Griger: in *International Workshop on the Effect of Iron and Silicon in Aluminium and its Alloys*, May 1989, Trans Tech Publishing, Zurich, Switzerland, Balatonfured, Hungary, 1990, pp. 57-67.
41. K.Y. Wen, W. Hu, and G. Gottstein: *Mater. Sci. Tech.*, 2003, vol. 19 (6), pp. 762-68.
42. M.V. Kral, M.H. R, and M.J. Smillie: *Scripta Mater.*, 2004, vol. 51 (3), pp. 215-19.
43. D.B. Williams and C.B. Carter: *Transmission Electron Microscopy*, Plenum Press, New York, N.Y., 1996.
44. M.H. Loretto: *Electron Beam Analysis of Materials*, Chapman and Hall, London, U.K., 1984.
45. J.C.H. Spence and J.M. Zuo: *Electron Microdiffraction*, Plenum Press, New York and London, 1992.
46. B.F. Buxton, J.A. Eades, J.W. Steeds, and G.M. Rackham: *Philos. Trans. R. Soc. London*, 1976, vol. 281A (1301), p. 171.
47. T. Hahn, ed.: *International Tables for Crystallography*, D. Reidel Publishing Co., Dordrecht, Holland/Boston, MA, U.S.A., 1983.
48. H.R. McIntyre, J. Looij, and M.V. Kral: in *Symposium on Solidification of Aluminum Alloys*, TMS Annual Meeting, M.G. Chu and D.A. Granger, eds., TMS, Charlotte, NC, U.S.A., 2004, pp. 111-20.
49. N.C.W. Kuipers, W.H. Kool, P.T.G. Koenis, K.E. Nilsen, I. Todd, and S. van der Zwagg: *Mater. Charact.*, 2003, vol. 49, pp. 409-20.
50. C.H. Caceres, C.J. Davidson, J.R. Griffiths, and Q.G. Wang: *Metall. Mater. Trans.*, 1999, vol. 30A, pp. 2611-18.
51. S.G. Shabestari and J.E. Gruzleski: *Trans AFS*, 1995, vol. 103, p. 285.
52. C.J. Simensen, P. Fartum, and A. Andersen: *Fresenius Z. Anal. Chem.,* 1984, vol. 319, pp. 286-92.
53. N.C.W. Kuipers, F.J. Vermolen, C. Vuik, P.T.G. Koenis, K.E. Nilsen, and S. van der Zwaag: *Mater. Sci. Eng.*, 2005, vol. 394, pp. 9-19.
54. M. Warmuzek, G. Mrowka, and J. Sieniawski: *J. Mater. Process. Technol.*, 2004, vol. 157–158, pp. 624-32.
55. M.V. Kral: *Mater. Lett.*, 2005, vol. 59 (18), pp. 2271-76.